Green's Function of Metasurface-Assisted Cavities

A. Torabi(1), G. Gradoni*(1)
(1) Institute for Communication Systems (ICS), 6G Innovation Centre
University of Surrey, Guildford GU2 7XH, U.K
e-mail: g.gradoni@surrey.ac.uk.

Abstract

An efficient and fast approach is presented for closed-form evaluation of the spatial domain Green's function for a 2D rectangular room. The room comprises a metasurface and dielectric walls. The characteristic Green's function (CGF) technique, separability assumption and generalized sheet transition condition are used to find a closed-form relation for magnetic vector potential Green's function of vertical electric dipole (normal to metasurface wall). The advantage of the proposed CGF-CI method lies in its speed due to independence from source and field point locations as well as its accuracy.

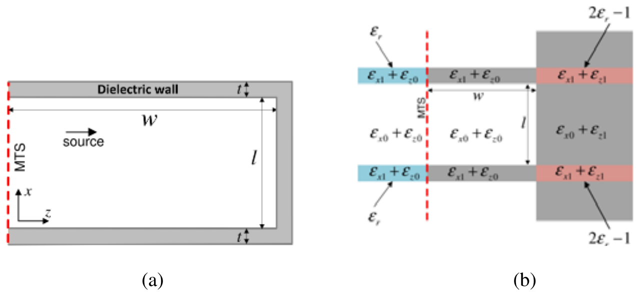

Figure 1. (a) MTS-assisted room and (b) separable structure analyzed in CGF technique instead of (a).

1 Introduction

Metamaterials have attracted significant attention due to their privileged characteristics which are widely used in antennas, filters, photonic bandgap (PBG) structures, etc. One layer of electrically thin metamaterials called metasurfaces (MTSs) can modify and enhance the propagation and radiation characteristics by working as reconfigurable intelligent surfaces (RISs) [1]. Considerable attention has been given to the plane wave interaction with MTSs [2]. MTS is modeled as a two-dimensional surface with equivalent electric and magnetic susceptibility dyadics and the related discontinuity in the electromagnetic field can be most generally described by generalized sheet transition conditions (GSTC) [3]. Great computational resources as well as the complexity of formulations are the main challenges of full-wave approaches like array scanning method utilized for aperiodic source placed near a planar peiodic surface [4], and also finite element method (FEM) [5] in indoor environments. But having the Green's function of the desired structure (i.e. empty room equipped by MTS) can drastically decrease the time of simulation while the accuracy is also preserved. The electric field dyadic Green's function for dipole excitation MTS was first presented by Liang *et al* [6] with the use of both surface impedance and surface susceptibility method for electric field integral equation (EFIE) formulation. However, the structures studied in [6] and other similar researches were a metafilm in free space and those cannot be effective in finite 2D room structure. In this paper, the CGF technique [7] is used to find a closed-form relation for magnetic vector potential Green's function of vertical electric dipole (VED) excitation (normal to MTS wall) in dielectric cavity shown in Fig. 1(a) that includes one MTS wall while other walls are considered dielectric slabs. The MTS includes a periodic array of planar scatterers and is replaced by a thin sheet with equivalent electric and magnetic surface susceptibility dyads. It is shown that the separation process in the CGF technique can be implemented by homogenization via GSTC for VED excitation. The CI method is used to approximate the spectral domain Green's functions as a sum of exponential terms, which leads to a closed-form mathematical expression of the spatial domain Green's function obtained by separability assumption. The expression is validated by full-wave simulations obtained in COMSOL. Excellent agreements have been obtained for various scenarios of source and field point locations and MTS characteristics.

2 CGF technique

Consider z-directed electric dipole source in a 2D structure like Fig. 1(a) (i.e. no variation in the y-direction) surrounded by layered media in both x and z direction. Magnetic vector potential Green's function satisfies inhomogeneous 2D Helmholtz's equation:

$$[\nabla_t^2 + k_0^2 \varepsilon_r(x,z)] G_z(x,z;x',z') = -\delta(x-x')\delta(z-z') \quad (1)$$

where $\nabla_t^2 \equiv \frac{\partial^2}{\partial x^2} + \frac{\partial^2}{\partial z^2}$, k_0 is the wave number of free space and (x',z') and (x,z) are the source and field points locations respectively. More, $\varepsilon_r(x,z)$ represents the relative dielectric constant of the medium. Now if the $\varepsilon_r(x,z)$ can be written as:

$$\varepsilon_r(x,z) = \varepsilon_x(x) + \varepsilon_z(z) \tag{2}$$

then it can be shown that the 2D Helmholtz's equation (1) can be separated into two 1D equations and $\varepsilon_\gamma(\gamma)$, $\gamma = x, z$ in (2) represents the relative dielectric constant in a layered media stratified normal to the γ-direction, denoted by $\mathscr{N}_\gamma$. The Green's function of each $\mathscr{N}_\gamma$ layered media is called characteristic Green's function (CGF) of the related $\mathscr{N}_\gamma$ media satisfies the following 1D Helmholtz's equation:

$$\frac{d^2\tilde{G}_\gamma}{d\gamma^2} + (\varepsilon_\gamma(\gamma)k_0^2 + \lambda_\gamma)\tilde{G}_\gamma = -\delta(\gamma - \gamma'), \tag{3}$$

where $\gamma = x, z$ and $\lambda_x + \lambda_z = 0$. $\tilde{G}_\gamma$ satisfies the appropriate boundary conditions of the 1D structure, $\mathscr{N}_\gamma$, only (sign tilde denotes the spectral domain). Once the CGFs of related $\mathscr{N}_\gamma$ media are available, the Green's function solution of (1) is given by contour integration of (4) where C_γ is the integration contour which encloses *only* the singularities of $\tilde{G}_\gamma$, including branch cuts, branch points and discrete pole singularities in the counterclockwise sense.

$$G_z(x,z;x',z') = \left(\frac{-1}{2\pi j}\right) \oint_{C_{\lambda_z}} G_x(x,x',\lambda_z) G_z(z,z',\lambda_z) d\lambda_z \tag{4}$$

Equation (2) is the main criterion for separability of a structure. If equation (2) is satisfied exactly, means that the original structure is decomposed exactly into $\mathscr{N}_\gamma$ media, and it is called *separable* and the exact analytical solution of Green's function can be obtained by (4). Otherwise, the structure is called *nonseparable*, and the integral of (4) would be an approximate solution for the original structure. Now one can consider the Fig. 1(a) as a 2D room with length l and width w with z-directed electric dipole source. But for simplicity of derivations, the wall in front of the MTS wall is considered as a dielectric region with infinite thickness, and the remaining two parallel walls normal to $\hat{x}$-direction are considered as dielectric slabs with thickness t. All dielectric regions are considered to have the same dielectric constant, ε_r, while the solution for different ε_r is straightforward. Inside the room is considered as free space ($\varepsilon = \varepsilon_0$). The MTS-assisted room of Fig. 1(a) is separated into 1D layered media shown in Fig. 2. The related dielectric constants of each region of $\mathscr{N}_x$ and $\mathscr{N}_z$ media are considered as $\varepsilon_{x0} = 0$, $\varepsilon_{x1} = \varepsilon_r - 1$, $\varepsilon_{z0} = 1$ and $\varepsilon_{z1} = \varepsilon_r$. In fact for MTS-assisted room of Fig. 1(a), it can be proved that the separation condition (2) cannot be exactly satisfied for all regions achieved by recombination of $\mathscr{N}_x$ and $\mathscr{N}_z$ media. Therefore, by ignoring the separation condition for four regions shown in Fig. 1(b), the approximate 2D structure of Fig. 1(b) is obtained for the original structure of Fig. 1(a). In this way, these outer regions are replaced by dielectric constants $2\varepsilon_r - 1$ and ε_r for right and left corners respectively. Actually source and field points are rarely placed in the proximity of these regions inside the room and therefore it is expected that these deviations in modeling do not matter much in communication and propagation channel issues. In Fig. 2(b), the $z > w$ region is replaced by a dielectric region which leads to the continuity of tangential components of the electric and magnetic field at $z = w$.

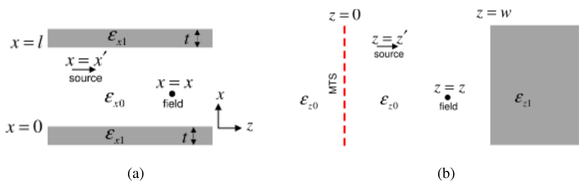

Figure 2. Separation of Fig. 1a to (a) $\mathscr{N}_x$ with $\varepsilon_{x0} = 0$, $\varepsilon_{x1} = \varepsilon_r - 1$ and (b) $\mathscr{N}_z$ with $\varepsilon_{z0} = 1$ and $\varepsilon_{z1} = \varepsilon_r$.

The proposed form of $\tilde{G}_z$ for VED source and field points located in region $0 < z < w$, is given below:

$$\tilde{G}_z(z,z',\lambda_z) = \begin{cases} \frac{e^{-jk_{z0}|z-z'|}}{2jk_{z0}} + R_{zz}^t e^{-jk_{z0}(w-z)} & \\ +R_{zz}^b e^{-jk_{z0}z} & 0 < z < w \\ T_{zz}^t e^{jk_{z0}z} & z < 0 \\ T_{zz}^b e^{-jk_{z1}(z-w)} & z > w \end{cases} \tag{5}$$

where $k_{zi} = \sqrt{\varepsilon_{zi}k_0^2 + \lambda_z}$, $(i = 0, 1)$ (according to separation, selected dielectric constants are: $\varepsilon_{z0} = 1$, $\varepsilon_{z1} = \varepsilon_r$) and R_{zz}^t and R_{zz}^b are the reflection of wave from top and bottom interfaces ($z = w$ and $z = 0$). Now applying GSTC for $z = 0$ and continuities of tangential components of fields at $z = w$, one can reach (6) for R_{zz}^b and R_{zz}^t. For avoiding prolongation, the relations for T_{zz}^t and T_{zz}^b are not given due to focusing on the fields of the inside of the room.

$$R_{zz}^t = \frac{R_d \chi_{ES}^{xx} e^{-jk_{z0}(w-z')} + R_d(2 + jk_{z0}\chi_{ES}^{xx})e^{-jk_{z0}(w+z')}}{2(2 + jk_{z0}\chi_{ES}^{xx} - jk_{z0}R_d\chi_{ES}^{xx}e^{-jk_{z0}2w})} \tag{6a}$$

$$R_{zz}^b = \frac{jk_{z0}\chi_{ES}^{xx}(R_d e^{-jk_{z0}(2w-z')} + e^{-jk_{z0}z'})}{2(2 + jk_{z0}\chi_{ES}^{xx} - jk_{z0}R_d\chi_{ES}^{xx}e^{-jk_{z0}2w})} \tag{6b}$$

In (6a) and (6b), χ_{ES}^{xx} are general xx component of electric surface dyad. We consider the shape and arrangement of components of metafilms that the related surface susceptibility dyads are diagonal. Moreover, we added the symmetrically of the physical structure in x and y directions. More, $R_d = \frac{\varepsilon_r k_{z0} - k_{z1}}{\varepsilon_r k_{z0} + k_{z1}}$ is the reflection coefficient of a TM wave at the interface of two regions in $\mathscr{N}_z$ medium of Fig. 2(b) at $z = w$. For the $\mathscr{N}_x$ medium shown in Fig. 2(a), one can find the closed-form expression of $\tilde{G}_x$ with the use of spectral domain technique:

$$\tilde{G}_x = \frac{e^{-jk_{x0}(|x-x'|)}}{2jk_{x0}} + \frac{R_x\left(e^{-jk_{x0}(x+x')} + e^{-jk_{x0}(2l-x-x')}\right)}{2jk_{x0}\left(1 - R_x^2 e^{-j2k_{x0}l}\right)} + \frac{R_x^2 e^{-j2k_{x0}l}\left(e^{jk_{x0}|x-x'|} + e^{-jk_{x0}|x-x'|}\right)}{2jk_{x0}\left(1 - R_x^2 e^{-j2k_{x0}l}\right)} \tag{7}$$

$$R_x = \frac{r_x - r_x e^{-j2k_{x1}t}}{1 - r_x^2 e^{-j2k_{x1}t}}, \; r_x = \frac{k_{x1} - k_{x0}}{k_{x1} + k_{x0}} \tag{8}$$

where $k_{xi} = \sqrt{\varepsilon_{xi}k_0^2 + \lambda_x}$, $(i = 0, 1)$ (according to separation: $\varepsilon_{x0} = 0$, $\varepsilon_{x1} = \varepsilon_r - 1$). Both spectral representations of $\tilde{G}_x$ and $\tilde{G}_z$ in (7) and (5) are in suitable forms for the

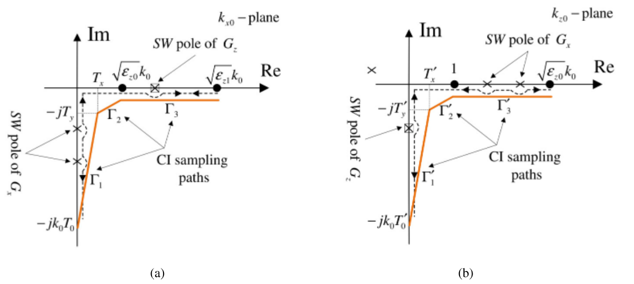

Figure 3. Integration path of CGF integration (a) in k_{x0} plane and (b) in k_{z0} plane after CI approximation of $\tilde{G}_x$.

CI approximation step to reach efficient spatial domain approximation. One can reach possible SW poles of $\tilde{G}_z$ by setting the denominator of (5) to zero, which leads to:

$$1 - R_d e^{-j2k_{z0}^{\mathrm{SW}} w} = \frac{-2}{jk_{z0}^{\mathrm{SW}} \chi_{ES}^{xx}} \tag{9}$$

It can be shown that $\chi_{ES}^{xx} < 0$ (exactly $\mathrm{Re}(\chi_{ES}^{xx}) < 0$)) is mandatory to have possible TM SW pole.

3 Closed-form derivation of spatial domain Green's function

Numerical computation of (4) is time-consuming due to the slowly convergent and oscillatory behavior of the integrand near the singularity. To circumvent this integration, CI analysis is utilized. Fig.3(a) shows the equivalent path of integration in k_{x0} plane ($k_{x0} = \sqrt{-\lambda_z}$) determined in dashed line. To perform three-level CI method the deformed path is shown in three pieces of the solid line in Fig.3(a). The required samples for three-level complex images are taken from these paths (Γ_1, Γ_2, and Γ_3 which are controlled by T_x, T_y, and T_0). Now to preserve the spatial dependencies, the location invariant part of $\tilde{G}_x$ is approximated by exponential series with the use of generalized pencil of function (GPOF) [8] in the following form:

$$\frac{R_x^i}{1 - R_x^2 e^{-j2k_{x0}l}} = \sum_{n=1}^{M_{xi}} c_n^{(i)} e^{k_{x0} d_n^{(i)}} \tag{10}$$

The approximate exponential series can be placed instead of the left terms of (10) in $\tilde{G}_x$ in (7). Then the integration plane of (4) is changed from λ_z-plane to λ_x-plane and the equivalent of the integration path in k_{z0} plane depicted in Fig. 3(b). For $\tilde{G}_z$ in (5), (6) is approximated in terms of exponentials over the deformed path depicted in Fig. 3 using three-level CI method. Again here we expand the location-invariant parts of Green's function $\tilde{G}_z$ in the following form:

$$\frac{F^{(i)}(k_{z0})}{2 + jk_{z0}\chi_{ES}^{xx}\left(1 - R_d e^{-j2k_{z0}w}\right)} = \sum_{m=1}^{M_{zi}} a_m^{(i)} e^{k_{z0} b_m^{(i)}} \tag{11}$$

where $i = 1,2,3$ and:

$$F^{(1)}(k_{z0}) = jk_{z0} R_d \chi_{ES}^{xx} \tag{12a}$$

$$F^{(2)}(k_{z0}) = (2 + jk_{z0}\chi_{ES}^{xx}) R_d \tag{12b}$$

$$F^{(3)}(k_{z0}) = jk_{z0}\chi_{ES}^{xx} \tag{12c}$$

it should be noted that expansion coefficients $(a_m^{(i)}, b_m^{(i)})$ for $i = 1,2,3$ are comprised by expansion coefficients of three paths (Γ_1', Γ_2' and Γ_3' in Fig. 3(c)) in three-level CI approximation. The advantage of expansion the location invariant parts of the CGFs ($\tilde{G}_x$ and $\tilde{G}_z$) with exponential terms is that CI approximation step may be performed *just once*. Now by inserting the exponential sum approximation of (10) and (11) in $\tilde{G}_x$ and $\tilde{G}_z$ respectively in the CGF integration (4), one can use the well-known Weyl's identity for the updated integral and then reach to closed-form derivation:

$$\begin{aligned} G_z(x,z,x',z') = \frac{1}{4j}\Bigg[& H_0^{(2)}\left(k_0\rho_{0,0}\right) + \sum_{m=1}^{M_{z1}} a_m^{(1)} H_0^{(2)}\left(k_0\rho_{0,m}^{21}\right) + \\ & \sum_{n=1}^{M_{xi}}\sum_{i=1}^{2}\sum_{j=1}^{2} c_n^{(i)} H_0^{(2)}\left(k_0\rho_{n,0}^{ji}\right) + \sum_{m=1}^{M_{zp}}\sum_{p=1}^{3} a_m^{(p)} H_0^{(2)}\left(k_0\rho_{0,m}^{1p}\right) + \\ & \sum_{n=1}^{M_{xi}}\sum_{m=1}^{M_{zp}}\sum_{i=1}^{2}\sum_{p=1}^{3}\sum_{j=1}^{2} a_m^{(p)} c_n^{(i)} H_0^{(2)}\left(k_0\rho_{n,m}^{ji,1p}\right) + \\ & \sum_{n=1}^{M_{xi}}\sum_{m=1}^{M_{z1}}\sum_{i=1}^{2}\sum_{j=1}^{2} a_m^{(1)} c_n^{(i)} H_0^{(2)}\left(k_0\rho_{n,m}^{ji,21}\right) \Bigg] \end{aligned} \tag{13}$$

where $\rho_{n,m}^{ji,pq} = \sqrt{\left(X_n^{ji}\right)^2 + \left(Z_m^{pq}\right)^2}$ for $n,m \neq 0$, $\rho_{0,m}^{pq} = \sqrt{\left(x-x'\right)^2 + \left(Z_m^{pq}\right)^2}$ for $n = 0, m \neq 0$, $\rho_{n,0}^{ji} = \sqrt{\left(X_n^{ji}\right)^2 + \left(z-z'\right)^2}$ for $n \neq 0, m = 0$ and $\rho_{0,0} = \sqrt{\left(x-x'\right)^2 + \left(z-z'\right)^2}$ for $n = 0, m = 0$. where:

$$X_n^{ji} = \begin{cases} X_n^{11} = x + x' + jd_n^{(1)} \\ X_n^{21} = 2l - x - x' + jd_n^{(1)} \\ X_n^{12} = 2l - |x - x'| + jd_n^{(2)} \\ X_n^{22} = 2l + |x - x'| + jd_n^{(2)} \end{cases} \tag{14}$$

$$Z_m^{pq} = \begin{cases} Z_m^{11} = 2w - z - z' + jb_m^{(1)} \\ Z_m^{21} = 2w + z - z' + jb_m^{(1)} \\ Z_m^{12} = 2w - z - z' + jb_m^{(2)} \\ Z_m^{13} = z + z' + jb_m^{(3)} \end{cases} \tag{15}$$

4 Simulation results

In this section, the derived closed-form relations for G_z of VED (z-directed) for studied structure is evaluated and examined. For structure shown in Fig.1(a), $w = 20.2\lambda$ and $l = 16.4\lambda$ are considered in simulations. The walls have thickness $t = 0.8\lambda$ and $\varepsilon_r = 3.75 - j0.28$ (this is a relative dielectric constant of a brick wall at 2.4 GHz) is considered). For susceptibility (χ_{ES}^{xx}) of MTS used in (6), one can use the concept of polarizability of any individual scatterer, that relates the dyad elements to dipole interaction assumption between elements described in [3]. For CI approximation steps in (10) and (11), $M_{t,i} = M_{t,i}^{(1)} + M_{t,i}^{(2)} + M_{t,i}^{(3)}$, ($t = x,z$), where $i = 1,2$ for $t = x$ and $i = 1,2,3$ for $t = z$, indicates the required number of images need to be extracted

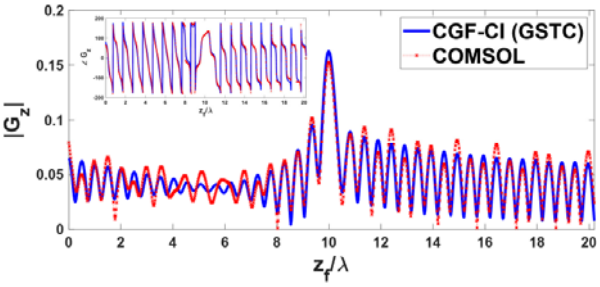

Figure 4. Amplitude and phase distributions of G_z with proposed CGF-CI and COMSOL for MTS-assisted room with $\chi_{ES}^{xx} = 0.1\lambda$. VED source is located at $(x_s, z_s) = (8.2\lambda, 10.1\lambda)$ and field points are considered at line $x_f = 7.7\lambda$ for different z_f.

in three-level CI corresponding to paths Γ_1, Γ_2 and Γ_3 for (10) related to $\mathscr{N}_x$ media and paths Γ_1', Γ_2' and Γ_3' for (11) related to $\mathscr{N}_z$ media (typically 10 to 20 images are sufficient for each path). Moreover, for the GPOF algorithm in each path, 50 to 250 sample points are required to achieve an error of less than 1%. For verification of the derived closed-forms and validation of the results, full wave simulations with the use of the COMSOL multiphysics tool are utilized. To verify and validate the accuracy of the closed-form relation (13), let's consider the results of amplitude and phase for G_z for the VED source located at the midpoint of the room $x_s = 8.2\lambda$ and $z_s = 10.1\lambda$. Fig. 4 shows the results for set of field points at lines $x_f = 7.7\lambda$ ($z_f \in [0, 20.2\lambda]$). Excellent agreements with the results of full-wave simulation are obtained while small deviations can be seen near the edges that comes from the separability assumption of the original structure and modeling it with separable one as well as considering the wall at $z = w$ as infinite extent dielectric region instead of dielectric slab. Larger values of field around the source point is clearly seen in Fig. 4. The derived closed-form evaluation is worth comparing with the ordinary real-world rooms with all-dielectric slab walls. For this room (which is nonseparable), all the details of closed-form derivations including separation step and using of CGF-CI technique are shown in [9] for VED excitation. Fig. 5 shows this experiment for field points distributed inside the room for VED located at $x_s = 8.2\lambda$ and $z_s = 5\lambda$. Fig. 5(a) shows the results of $|G_z|$ for ordinary room while Fig. 5(b) and show the same simulation for MTS-assisted room (MTS at $z = 0$). It is clear that by using MTS, improvement in field intensity is achieved. It is proved and shown that this improvement is very dominant for MTS with $\chi_{ES}^{xx} < 0$ due to surface wave presenc.

5 Conclusions

An efficient GF analysis approaches is presented with the use of CGF technique for a MTS-assisted room. A closed-form expression is derived by separation operation and evaluation of spectral domain GF of 1D layered media with applying GSTC boundary condition for MTS wall. The advantage of the proposed method lies in its speed due to independence from source and field point locations as well as its accuracy. Excellent agreements have been obtained for various scenarios in comparison with COMSOL results.

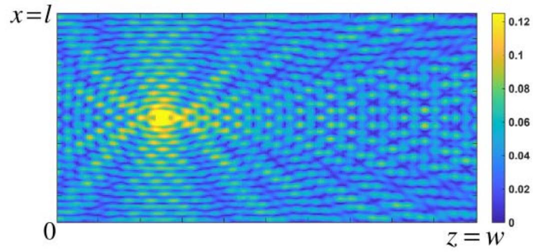

(a)

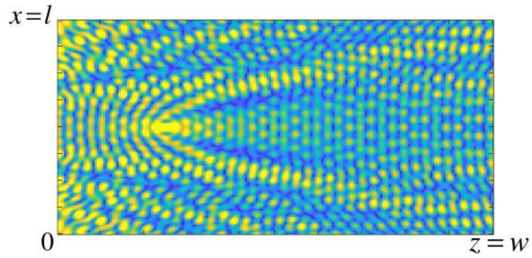

(b)

Figure 5. Amplitude of G_z with proposed CGF-CI method for (a) ordinary room with dielectric slab walls in [9] and (b) MTS-assisted room with () with $\chi_{ES}^{xx} = -0.1\lambda$.

References

[1] C. Ross, G. Gradoni, Q. J. Lim, and Z. Peng, "Engineering reflective metasurfaces with ising hamiltonian and quantum annealing," *IEEE Transactions on Antennas and Propagation*, vol. 70, no. 4, pp. 2841–2854, 2021.

[2] V. Tiukuvaara, T. J. Smy, K. Achouri, and S. Gupta, "Surface susceptibilities as characteristic models of reflective metasurfaces," *IEEE Transactions on Antennas and Propagation*, vol. 70, no. 11, pp. 10 583–10 591, 2022.

[3] E. F. Kuester, M. A. Mohamed, M. Piket-May, and C. L. Holloway, "Averaged transition conditions for electromagnetic fields at a metafilm," *IEEE Transactions on Antennas and Propagation*, vol. 51, no. 10, pp. 2641–2651, 2003.

[4] G. Lovat, R. Araneo, S. Celozzi *et al.*, "Electromagnetic shielding of resonant frequency-selective surfaces in presence of dipole sources," *ACES Journal*, vol. 29, no. 7, pp. 442–450, 2014.

[5] S. Sandeep, J.-M. Jin, and C. Caloz, "Finite-element modeling of metasurfaces with generalized sheet transition conditions," *IEEE Transactions on Antennas and Propagation*, vol. 65, no. 5, pp. 2413–2420, 2017.

[6] F. Liang, G. W. Hanson, A. B. Yakovlev, G. Lovat, P. Burghignoli, R. Araneo, and S. A. H. Gangaraj, "Dyadic Green's functions for dipole excitation of homogenized metasurfaces," *IEEE Transactions on Antennas and Propagation*, vol. 64, no. 1, pp. 167–178, 2015.

[7] A. Torabi, A. A. Shishegar, and R. Faraji-Dana, "An efficient closed-form derivation of spatial Green's function for finite dielectric structures using characteristic Green's function-rational function fitting method," *IEEE Transactions on Antennas and Propagation*, vol. 62, no. 3, pp. 1282–1292, 2013.

[8] Y. Hua and T. Sarkar, "Generalized pencil-of-function method for extracting poles of an EM system from its transient response," *IEEE Trans. Antennas Propag.*, vol. 37, no. 2, pp. 229 –234, Feb 1989.

[9] M. H. Sadrearhami and A. A. Shishegar, "Closed-form Green's function of a 2-d rectangular room," *IEEE Transactions on Antennas and Propagation*, vol. 64, no. 12, pp. 5291–5298, 2016.